Research Article

Valorization of Lignin-Rich Meranti (*Shorea* sp.) Sawdust into Cellulose Nanocrystals via APS Pretreatment: A Severity Map and Operating Window

Amun Amri*, Dewi Sutriani, Irene Olyvia Sirait, Chairul and Syelvia Putri Utami
Department of Chemical Engineering, University of Riau, Pekanbaru, Indonesia

Hatem Taha and Hussein Ali Miran
Department of Physics, College of Education for Pure Science, Ibn Al-Haitham, University of Baghdad, Baghdad, Iraq

Mohammad Mahbubur Rahman
Department of Physics, Jahangirnagar University, Savar, Dhaka, Bangladesh

Khairulazhar Jumbri
Department of Fundamental and Applied Sciences, Universiti Teknologi Petronas, Malaysia

Zhong Tao Jiang
Surface Analysis and Materials Engineering Research Group, College of Science, Health, Engineering and Education, Murdoch University, Murdoch, WA, Australia

* Corresponding author. E-mail: amun.amri@eng.unri.ac.id DOI: 10.14416/j.asep.2026.05.002
Received: 27 December 2025; Revised: 7 February 2026; Accepted: 11 March 2026; Published online: 12 May 2026

Abstract
Developing routes to produce cellulose nanocrystals (CNCs) from high-lignin wood residues is essential for expanding sustainable nanocellulose feedstocks. In this work, Meranti (*Shorea* sp.) sawdust was valorized into CNCs by integrating ammonium persulfate (APS) pretreatment with subsequent sulfuric acid hydrolysis. To establish a severity map and define an operating window, APS pretreatment severity was systematically varied by adjusting APS concentration and the sawdust-to-APS (solid-to-liquid) ratio, and its influence on CNC structural properties was evaluated. APS pretreatment partially disrupted and oxidized the lignocellulosic matrix, enabling acid hydrolysis to liberate crystalline cellulose domains. XRD analysis confirmed the preservation of the cellulose I crystalline structure, with a maximum crystallinity index of 72% at 2 M APS and a sawdust-to-APS ratio of 1:30 (w/v), and an average crystallite size of approximately 10 nm estimated using the Scherrer equation. SEM and TEM analyses revealed rod-like CNCs with smooth surfaces and relatively homogeneous dimensions. The optimized samples exhibited CNC lengths of 188.71 ± 5.01 nm and widths of 26.79 ± 1.72 nm. These results demonstrate that Meranti sawdust, a high-lignin wood residue, can be converted into structurally well-defined CNCs using a two-step APS/acid process without prior alkaline pulping or bleaching. This study clarifies the role of APS oxidation in enabling CNC production from feedstocks with lignin contents above 20% and provides a basis for valorizing Meranti sawdust as a renewable precursor for CNCs in advanced material applications.

Keywords: Ammonium persulfate oxidation, Cellulose nanocrystal, High-lignin biomass, Meranti sawdust (*Shorea* sp), Sulfuric acid hydrolysis

1 Introduction

Cellulose nanocrystals (CNCs) have emerged as a class of renewable nanomaterials with outstanding mechanical properties, high aspect ratios, large specific surface areas, and abundant surface hydroxyl groups that can be chemically modified [1]–[5]. These attributes make CNCs attractive for a broad range of applications, including polymer nanocomposites [6], lightweight epoxy composites reinforced with natural cellulosic fibers [7], functional coatings, water treatment, biomedical devices, food packaging, and drug delivery systems [2], [8], [9]. CNCs are commonly obtained from cellulose or lignocellulosic resources and typically exhibit a cellulose I crystalline structure with crystallinity indices above 50% and rod–like morphologies on the nanometre scale [5], [6], [8], [10].

Despite this potential, the production of CNCs at scale remains challenging. Conventional extraction routes frequently rely on multi–step pre–treatments, such as alkaline pulping and bleaching, followed by acid hydrolysis or oxidative treatments [5], [11]–[15]. These processes often require long reaction times, large amounts of chemicals, and significant energy input, which can limit their industrial viability and increase environmental burdens [11]–[14]. For example, two–step schemes that combine extensive delignification, bleaching, and subsequent mineral–acid hydrolysis may yield CNCs with high crystallinity but at the expense of complex operations and high chemical consumption [11]–[13]. Oxidative routes such as TEMPO–mediated oxidation offer efficient fibrillation and controlled surface functionalization, yet they can suffer from incomplete oxidation or require additional acid treatments to fully isolate crystalline cellulose domains, particularly when applied to lignocellulosic feedstocks with high lignin contents [6], [16], [17].

In parallel, there is increasing interest in valorising industrial and forestry residues as sustainable sources of nanocellulose. Wood sawdust (waste from the sawmill industry), agricultural by–products, and other lignocellulosic wastes represent abundant and underutilised biomass streams that could be upgraded into high–value CNCs [18], [19]. However, many of these residues contain substantial amounts of lignin and hemicellulose, which complicate CNC extraction and often necessitate harsh chemical pretreatments. In particular, high–lignin feedstocks tend to require more severe pulping and bleaching conditions or multiple sequential steps, further intensifying chemical and energy demands and generating large volumes of effluents [20]–[22].

Developing extraction strategies that can deal effectively with high lignin contents while minimising process complexity, therefore, remains an important challenge. Recent reviews of chemical pretreatments for lignocellulosic biomass highlight that pretreatment selection and severity strongly control recalcitrance reduction and downstream processing burdens, reinforcing the need for simplified yet effective strategies for high–lignin residues [23], [24]. Ammonium persulfate (APS) oxidation has recently attracted attention as an alternative or complementary step in CNC production [25], [26]. Under appropriate conditions, APS decomposes to generate strong oxidizing species capable of degrading lignin and hemicellulose while partially oxidizing cellulose surfaces, thereby facilitating the subsequent liberation of crystalline domains [27], [28]. APS–based treatments have been applied to various lignocellulosic substrates, including bamboo and other residues, often followed by additional steps, such as alkaline extraction or acid hydrolysis, to obtain CNCs [1], [16], [25]. These studies suggest that APS can simultaneously promote delignification and introduce surface functionalities, but they also indicate that process performance is highly sensitive to APS concentration, reaction temperature, and solid–to–liquid ratio [29]. Furthermore, the extent to which APS pre–oxidation can replace conventional pretreatments, particularly for high–lignin woody residues, remains insufficiently understood.

Beyond their sustainable origin, cellulose nanocrystals (CNCs) offer practical advantages for advanced materials due to their high crystallinity, high specific surface area, and rod–like morphology. In polymer nanocomposites, CNCs can act as reinforcing nanofillers that improve stiffness through load transfer and network formation, while in coatings and thin films they can contribute to uniform film formation and enhanced barrier performance. CNC suspensions can also function as rheological modifiers and stabilizers in water–based formulations because anisotropic nanoparticles can form percolated networks that increase viscosity and improve dispersion stability. These attributes have motivated the use of CNCs in applications ranging from composite reinforcement to coatings/packaging and functional aqueous formulations [30], [31].

Meranti (*Shorea* sp.) wood is widely used in the timber industry, particularly in Southeast Asia, and its processing generates substantial quantities of sawdust. Reported compositions indicate that Meranti sawdust contains around 41.58% cellulose and a relatively high lignin content, making it a representative example of high–lignin wood residues with significant potential as a CNC precursor [32]. Nevertheless, the direct conversion of Meranti sawdust into CNCs is nontrivial because the high lignin fraction can hinder cellulose accessibility and limit the efficiency of purely acid–based hydrolysis routes. Existing studies on CNCs from hardwood species typically rely on extensive alkaline pulping and bleaching prior to hydrolysis, which increases process complexity and chemical demand [33], [34]. More importantly, for high–lignin woody sawdust, there remains a limited systematic understanding of how APS pretreatment severity, particularly APS concentration and sawdust–to–APS ratio (solid–to–liquid ratio), controls CNC structural outcomes (crystallinity index and TEM–derived rod–like morphology). Without this correlation, an operating window that balances effective matrix disruption/delignification against the risk of over–oxidation (damage to ordered cellulose domains and reduced crystallinity) is not clearly established for lignin–rich sawdust feedstocks. To address these challenges, this study investigates the production of CNCs from Meranti sawdust using a two–step APS oxidation followed by sulfuric-acid hydrolysis, without prior alkaline pulping or bleaching. APS oxidation is applied to disrupt the lignocellulosic matrix and improve cellulose accessibility, after which sulfuric-acid hydrolysis releases the crystalline domains as CNCs. The effects of APS concentration and sawdust–to–APS ratio on CNC structure are systematically evaluated in terms of crystallinity (XRD/CI) and TEM–derived morphology. This work aims to assess Meranti sawdust as a high–lignin feedstock for CNC production without conventional pulping/bleaching, establish how APS severity controls crystallinity and particle dimensions, and identify processing conditions that yield well–defined CNCs for advanced material applications.

CNC production from high–lignin sawdust remains challenging because pretreatment severity must be balanced to promote delignification/ disruption while preserving ordered cellulose domains. The novelty of this work lies in establishing an operating window for a high–lignin feedstock (Meranti, ≈33.56% lignin), where moderate APS severity increases the relative crystalline contribution, whereas excessive severity reduces crystallinity, indicating the onset of oxidative damage. Under the optimized condition (2 M APS, 1:30 w/v), CNCs with cellulose I features, high crystallinity (72%), and rod–like nanoscale dimensions were obtained, supporting the feasibility of converting high–lignin sawdust into CNCs via a simplified route for advanced material development.

2 Materials and Methods

2.1 *Materials*

Meranti sawdust (*Shorea* sp.) was used as the raw material in this study. The sawdust was obtained from a sawmill industry located in Riau, Indonesia, with a lignin content of approximately 33.56% based on standard chemical composition analysis. High–lignin sawdust as a CNC feedstock presents inherent limitations related to feed variability and process reproducibility. Batch–to–batch variations in lignin/hemicellulose content, extractives, ash/ minerals, moisture, and particle–size distribution can change reagent demand and mass transfer during APS oxidation and subsequent acid hydrolysis, potentially affecting consistency of CNC quality. In addition, impurities such as resinous extractives and inorganic particulates may increase oxidant consumption, contribute to residual coloration, and complicate washing/neutralization. Consequently, strict control of raw–material preconditioning (e.g., drying to constant moisture, sieving to a defined particle size range, and periodic compositional checks) is recommended to improve reproducibility when using high–lignin sawdust–derived biomass.

Ammonium persulfate (APS) with 99% purity (Sigma–Aldrich, USA) was used in the experiment without further purification. 64% sulfuric acid (H_2SO_4, Merck, Germany) was employed for the acid hydrolysis process. All other chemicals used in this study were standard laboratory reagents, and deionized water was used to wash and stabilize the final product.

2.2 *APS oxidation and acid hydrolysis procedure*

The oxidation process [25] was carried out in a closed reactor by mixing Meranti sawdust with ammonium persulfate (APS) at sawdust–to–APS ratios of 1:20, 1:30, and 1:40 (w/v) and APS concentrations of 1, 2,

and 3 M. The ratios correspond to 20, 30, and 40 mL APS solution per gram of dried sawdust. Thus, the APS input spanned 0.02–0.12 mol per gram sawdust (4.56–27.36 g APS per gram sawdust, Mr = 228 g/mol), depending on concentration and liquid–to–solid ratio. The mixture was heated at 60 °C with a stirring speed of 300 rpm for 7 hours. After oxidation, the mixture was cooled and centrifuged at 7000 rpm for 15 minutes to separate the solvent from the precipitate. The supernatant was discarded, and the remaining pellet was transferred to a reactor containing 15 ml of 64% sulfuric acid and heated at 50 °C for 2 hours to promote preferential hydrolysis of disordered cellulose domains and facilitate CNC isolation.

After acid hydrolysis, 200 ml of deionized water was added to the reactor, and the mixture was centrifuged again. The washing process was repeated by alternating between washing, centrifugation, and sonication cycles to remove any remaining acid and optimize the quality of the CNC suspension. Washing was stopped when the pH of the solution reached approximately 6, with deionized water replaced three times over an 8 h period. This process aimed to obtain a clean and stable CNC suspension. These conditions determine reagent intensity and processing time and generate a sulfate–containing aqueous effluent from persulfate/acid usage and washing/neutralization, which is relevant to later assessment of scalability and economic viability.

2.3 *Characterization*

The CNCs produced from the APS oxidation and acid hydrolysis processes were then analyzed to determine their structural properties and morphology using various characterization techniques. One of the techniques employed was X–ray diffraction (XRD), which is useful for measuring the crystallinity index and crystallite size of the obtained CNCs. The XRD diffractogram was analyzed within the Bragg angle range (2θ) from 10° to 100°, using the XPERT–PRO Panalytical instrument (Panalytical Ltd., UK) operated at a temperature of 25 °C. This XRD analysis provided important information about the crystallinity level and structural characteristics of the produced CNCs. The crystallinity index (CI) of the nanocellulose fibers was calculated using Equation (1) [35], [36].

$$CI = \frac{I_{max} - I_O}{I_{max}} x\ 100\% \quad (1)$$

Where I_{max} represents the crystallinity peak's intensity and I_O is the minimum intensity at 2θ, indicating the amorphous region. Crystallite size determination was based on the central peak of the diffractogram pattern using the Debye–Scherrer equation, calculated with Equation (2) [36], [37].

$$D\ (nm) = \frac{K\lambda}{\beta \cos\theta} \quad (2)$$

Where K is the Scherrer constant (0.9), λ is the wavelength of the X–ray used (Cu, λ = 0.15406), β is the full width at half maximum (FWHM) (rad), and θ is the diffraction angle (rad). XRD data were collected at 25 ℃ over a Bragg angle (2θ) range from 10°-100°. At the primary peak of the diffractogram pattern, the value of Θ was found to be 0.0142 rad, and the FWHM was 0.2042 rad.

In addition, Scanning Electron Microscopy (SEM) was used to observe the surface morphology of the CNCs at high magnification, up to 20,000 times. This observation provided a visual representation of the shape, size, and distribution of the CNC particles produced. SEM was operated using a JEOL JCM 7000 SEM (JEOL Ltd., Japan), which enabled detailed visualization of the CNC surface, allowing us to assess the smoothness of the surface and the uniformity of particle size. For a more in–depth analysis of particle size and morphology at a higher resolution, Transmission Electron Microscopy (TEM) was employed. TEM provided a morphology view at the nanometer scale and was used to measure particle size and determine the uniformity of CNC dimensions. This technique was performed on a TEM HT7700 instrument (Hitachi High Technologies America, Inc., USA) with an acceleration voltage of 120 kV, providing the high resolution necessary to accurately and precisely analyze particle size.

3 Results and Discussion

3.1 *Morphological transformation of eranti sawdust and CNC purification process*

Figure 1 illustrates the morphological transformation of Meranti sawdust before and after treatment with ammonium persulfate (APS). Figure 1(a) shows untreated sawdust, while Figure 1(b) presents sawdust treated with 1 M APS. In this process, APS is used as an oxidative pretreatment intended to partially disrupt/solubilize lignin-associated structures and preferentially affect less–ordered (amorphous/

disordered) regions, thereby improving accessibility for the subsequent sulfuric–acid hydrolysis step, which releases crystalline domains as cellulose nanocrystals (CNCs). Oxidation with APS offers a significant advantage as it eliminates the need for alkali treatments or bleaching, which are commonly used in conventional methods that typically involve high chemical consumption and increase process complexity and chemical demand [29].

The APS oxidation process involves the decomposition of persulfate ions ($S_2O_8^{2-}$) under heat to generate free radicals (SO_4^{-}) that break down the strong lignin structure and oxidize the amorphous regions of cellulose, as shown in Equation (3). These free radicals, along with hydrogen peroxide (H_2O_2) formed under acidic conditions (pH 1.0) as described in Equation (4), open the aromatic rings of lignin and break down the amorphous regions of cellulose. This process leads to lignin degradation and the strengthening of the crystalline cellulose structure, as described in several previous studies [25].

$$S_2O_8^{2-} + heat \rightarrow 2SO_4^{\cdot -} \quad (3)$$

$$S_2O_8^{2-} + 2H_2O \rightarrow 2HSO_4^{-} + H_2O_2 \quad (4)$$

In the present dataset, the selective role of APS is supported by qualitative visual indicators (Figure 1) and severity–dependent crystallinity outcomes (section 3.3). Moderate APS severity increases the relative crystalline contribution, while excessive APS severity reduces crystallinity, indicating the onset of oxidative damage to ordered domains. Figure 1(b) shows that the yellow coloration remains after 1 M APS treatment, indicating that oxidative modification/solubilization of lignin–derived chromophores was incomplete at this concentration. Increasing the APS concentration to 2 M and 3 M (Figures 1(c) and 1(d)) produced progressively lighter coloration, which is interpreted as a qualitative indication of more extensive oxidation/solubilization of lignin-associated chromophores, rather than direct quantitative confirmation of complete lignin removal [1]. Importantly, this visual trend is consistent with increasing oxidative severity, which can also influence the disordered (amorphous) fraction and, at excessive severity, may begin to affect ordered cellulose domains (as reflected by the crystallinity decrease at 3 M, see section 3.2).

After APS oxidation, sulfuric acid hydrolysis was applied to isolate CNCs from APS–treated, cellulose–enriched solids. Figure 2 shows the CNCs after sulfuric acid treatment. While acid hydrolysis preferentially hydrolyzes disordered cellulose domains and facilitates the release of crystalline regions as CNCs [38], [39]. This study did not quantify residual lignin/hemicellulose after each intermediate step. Therefore, the product is described as CNC–rich/cellulose–enriched rather than completely lignin–free.

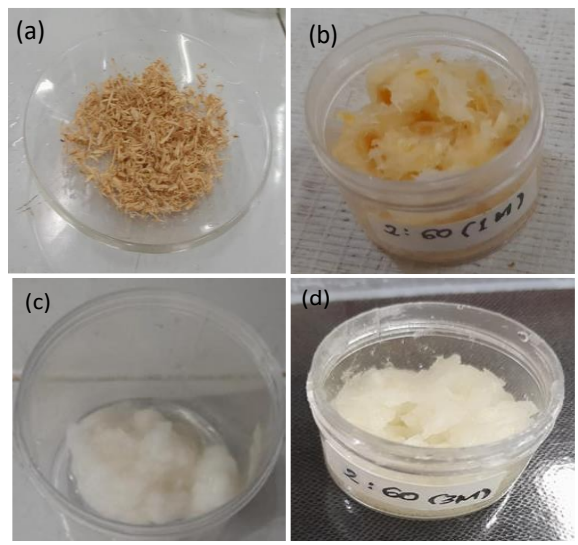

Figure 1: (a) Samples of sawdust before treatment, (b) After treatment with 1 M APS, (c) After treatment with 2 M APS, and (d) After treatment with 3 M APS.

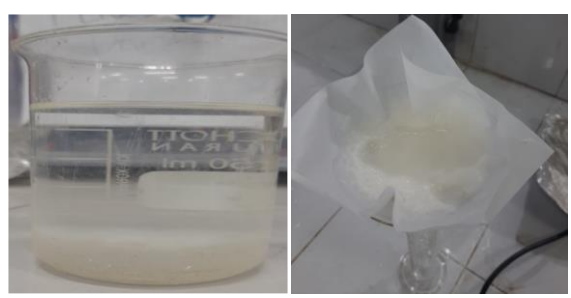

Figure 2: CNCs after sulfuric acid treatment.

3.2 *X–ray diffraction (XRD) analysis*

Figure 3 shows the X–ray diffraction (XRD) pattern of CNC samples produced through ammonium persulfate (APS) oxidation and acid hydrolysis. Each sample exhibits a primary peak in the 2θ range of 22.7°-23.4°, which aligns with the standard ICDD 00–056–1718 peak position for cellulose I_β, located at approximately 22.3° 2θ. This primary peak indicates that the CNCs

produced have a crystalline structure of cellulose I_β, which is the most stable and well–structured crystalline form of cellulose [1], [35], [36]. The presence of this primary diffraction peak suggests that the majority of the material produced is crystalline cellulose, which is highly desirable for nanomaterial applications.

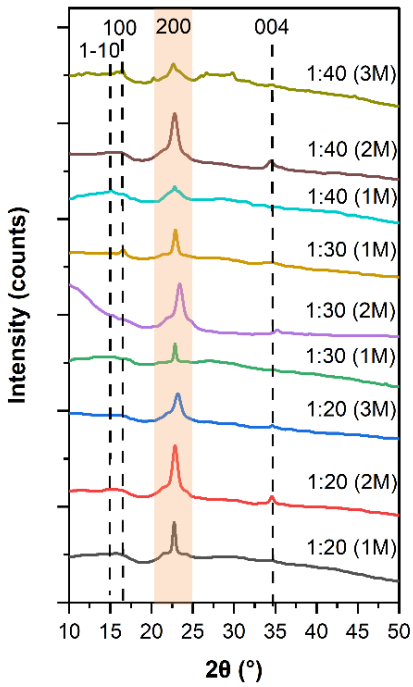

Figure 3: XRD spectra of CNCs in various sawdust–to–APS (w/v) ratios.

However, the smaller and less sharp peaks in the diffraction area (Figure 3) indicate the presence of amorphous phases in the samples. This suggests that while most of the cellulose remains structured, some material is not fully organized into crystalline form. The diffraction pattern also reveals characteristic peaks at 34.4°, 22.5°, 16.4°, and 14.6°, corresponding to the lattice planes 004, 200, 110, and 1–10, respectively. These peaks indicate the presence of cellulose I structure, which consists of parallel glucan chains (β–(1→4)–D–glucopyranose) that repeat, as described in previous literature [40], [41]. This cellulose I structure is important as it is the most commonly found form of cellulose in nature and exhibits good stability for various applications. Non–cellulosic polysaccharide bonds are detected in several samples, marked by the diffraction planes 004, 110, and 1–10, which are not clearly visible [40].

At an APS concentration of 2 M, the intensity and sharpness of the cellulose crystal peaks are higher compared to the APS concentrations of 1 M and 3 M, indicating a higher crystallinity at the 2 M concentration [35]. This increase in crystallinity suggests that APS oxidation at 2 M is more effective in removing lignin and amorphous regions from the cellulose structure, which, in turn, enhances the amount of crystalline regions in the CNCs. This is crucial because CNCs with high crystallinity exhibit superior mechanical and thermal properties, as well as better stability in nanomaterial applications [42–44].

However, at an APS concentration of 3 M, the diffraction peaks appear broader and the intensity is lower, indicating a decrease in crystallinity [35], [45]. This phenomenon suggests that at higher APS concentrations, degradation of the crystalline cellulose structure occurs due to excessive oxidation [1], [46]. Over–oxidation can damage the hydrogen bonds between cellulose chains that form the crystalline regions, leading to a decrease in crystallinity or even a transition to an amorphous form [47]. Therefore, although higher APS concentrations may be more efficient in removing lignin, they can cause damage to the crystalline cellulose structure, reducing the quality of the resulting CNCs.

Furthermore, the crystallite size calculation based on the Scherrer equation shows that at an APS concentration of 2 M, the crystallite size of the resulting CNCs is approximately 9.9 nm, which aligns with the observed increase in crystallinity [37]. The Scherrer–derived crystallite size (~9.9 nm) represents an apparent value from peak broadening and is used here as an indicative parameter. The estimated value, together with the sharp cellulose I reflections, suggests the presence of ordered crystalline domains relevant for polymer composites and coatings [48], [49]. The crystallite size estimated by the Scherrer equation should be considered an apparent crystallite size based on peak broadening. In the present analysis, instrumental broadening and microstrain were not independently corrected/separated. Therefore, the reported value may include contributions from these effects in addition to finite crystallite size. Accordingly, the Scherrer–derived crystallite size is used here only as a comparative/indicative parameter.

Table 1 shows the relationship between increasing APS concentration and the crystallinity degree of CNCs at various sawdust–to–APS ratios. The increase in APS concentration correlates with an increase in CNC crystallinity, with an average

increase of approximately 18%. This increase indicates that stronger oxidation, through higher APS concentrations, is more efficient in removing lignin, hemicellulose, and amorphous regions from the cellulose structure, contributing to the improvement of crystallinity [40], [50]. However, at an APS concentration of 3 M, the 17% decrease in crystallinity indicates degradation due to excessive oxidation, which damages the crystalline cellulose structure [1], [46]. Overall, an APS concentration of 2 M proved to be the optimal condition, producing CNCs with the highest crystallinity (72%) and the best quality. This result is higher than the CNC crystallinity of 69.8% reported by Hu *et al.*, [51] at the same concentration. For comparison with a conventional route (bleached pulp followed by sulfuric acid hydrolysis), Chen *et al.,* reported a Segal CrI of 76 % for the starting bleached eucalyptus kraft pulp and ~73% for CNC produced at 58 wt% H_2SO_4. H_2SO_4. Our maximum Segal CrI (~72%) is comparable to this conventional CNC crystallinity level, despite the use of a high–lignin sawdust feedstock and the absence of alkaline pulping/bleaching [52]. These findings align with previous reports that suggest the optimal APS concentration provides the best balance between lignin removal and the preservation of cellulose crystalline structure [29], [51].

Table 1: The relationship between increasing in APS concentration and CNC crystallinity degree in various sawdust–to–APS (w/v) ratios.

Sawdust:APS (w/v)	APS concentration (M)	Crystallinity index, CI (%)
1:20	1	47.20
1:20	2	57.39
1:20	3	50.94
1:30	1	48.13
1:30	2	71.97
1:30	3	41.07
1:40	1	31.73
1:40	2	55.43
1:40	3	41.44

3.3 *Scanning electron microscopy (SEM) analysis*

Figure 4 shows the Scanning Electron Microscopy (SEM) analysis results of raw Meranti sawdust. In Figures 4(a–b), the surface of the Meranti sawdust particles appears to contain cellulose fibers and fine aggregates [49]. This image shows that the Meranti sawdust consists of cellulose fibers ranging in size from approximately 1–10 µm, making it a suitable raw material for the production of cellulose nanocrystals (CNCs). Additionally, Figures 4(c–d) reveal the presence of disintegrated fibrils and cavities, indicating the breakdown or splitting of fibers through mechanical processes such as milling, cutting, or sanding [38]. This disintegration process suggests that Meranti sawdust contains fibers that can be further processed into CNCs with additional treatment [53].

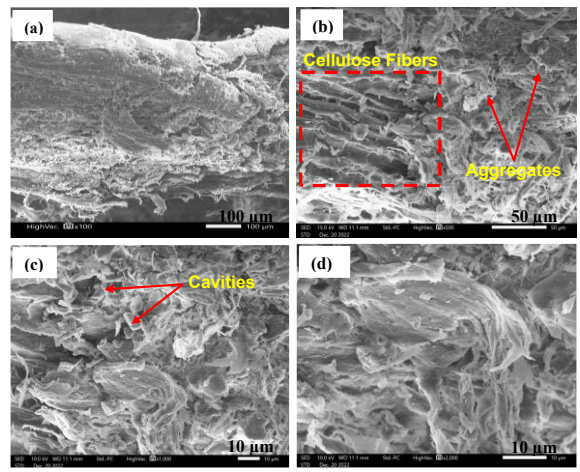

Figure 4: Morphology of Meranti sawdust at magnifications of (a) 100x, (b) 500x, (c) 1000x, (d) 2000x.

Figure 5 shows the morphology of CNCs after oxidation with ammonium persulfate (APS) at a concentration of 1 M and a sawdust–to–APS ratio of 1:40. In this image, it can be seen that the oxidation process successfully removed most of the fine aggregates from the cellulose fibers, resulting in a denser fiber structure. However, further analysis using ImageJ software revealed that the cellulose diameter after oxidation was approximately 2.4 µm. indicating much of the material remained aggregated. This aggregation is most likely due to suboptimal sonication, which hindered the effective dispersion of the CNC nanoparticles [54]. Therefore, although oxidation has transformed the cellulose structure into a denser form, it was not sufficient to produce nanocellulose with smaller sizes and a more uniform size distribution [55]. Regarding delignification uniformity, the present study provides only qualitative morphology evidence from SEM, which primarily reflects surface/near–surface changes. SEM images from representative regions show consistent matrix disruption after APS oxidation, suggesting broadly similar structural effects across observed particles. However, spatial uniformity of delignification

throughout the full biomass particle cross–section was not quantified here.

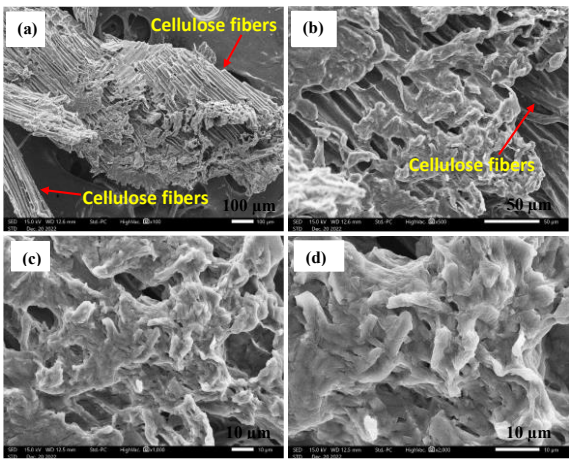

Figure 5: Morphology of CNCs post–oxidation process at magnifications of (a) 100x, (b) 500x, (c) 1000x, (d) 2000x.

Figure 6 shows the SEM results of CNCs after oxidation and acid hydrolysis, followed by 7 hours of stirring, centrifugation, and 15 minutes of sonication. In these images, it can be observed that the cellulose fibers consist of both crystalline and amorphous phases, with the crystalline phase being more dominant [56]. Figure 6(a)–(d) show that the breakdown of the cellulose fibers due to the removal of the amorphous regions is clearly visible, resulting in CNCs with a more homogeneous surface. Although most of the amorphous regions have been removed, microfibrillar cellulose structures are still visible, indicating that the acid hydrolysis process did not completely break down the amorphous structure of the wood cellulose fibers.

According to Vasconcelos *et al.*, [57], although acid hydrolysis produces cellulose nanocrystals (CNCs), incomplete breakdown of the amorphous structure can result in nanocrystals larger than 100 nm [57]. This is related to the short hydrolysis time, which hinders the breakdown of the amorphous phase in wood cellulose fibers [58]. Longer hydrolysis times can degrade most of the amorphous structure and increase the crystallinity of the resulting CNCs [59]. As seen in Figure 6, the fibers in the CNCs exhibit aggregation, forming micrometer–sized fibers due to strong hydrogen bonds between cellulose chains and stable Van der Waals forces between glucose molecules [60], [61].

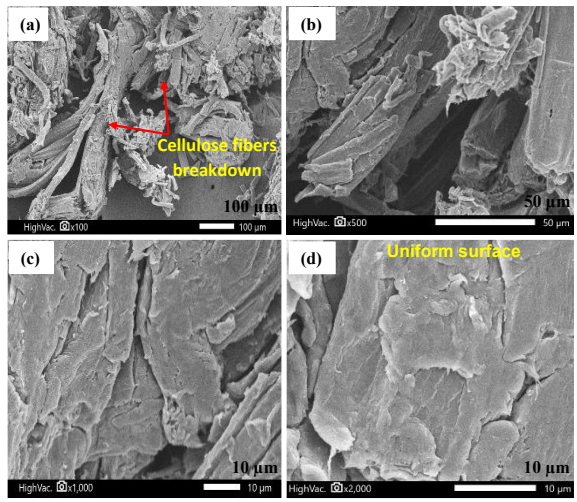

Figure 6: Morphology of CNCs after acid hydrolysis process at magnifications of (a) 100x, (b) 500x, (c) 1000x, (d) 2000x.

The incomplete lignin decomposition and the presence of minerals such as ash and silica in Meranti wood also affect the lignin decomposition process, which in turn influences the fiber size distribution in the CNCs. Incomplete lignin decomposition results in an uneven fiber size distribution, leading to larger CNC particle sizes and a broader size distribution [62]. Therefore, additional processes such as mechanical treatment using an ultrasonicator and mechanical grinding are essential to achieve smaller CNC sizes and a narrower size distribution. Combining physical and chemical methods can provide an alternative approach to improving the efficiency of the nanocellulose isolation process [62].

3.4 *Transmission Electron Microscopy (TEM) analysis*

Figure 7 shows the Transmission Electron Microscopy (TEM) analysis results of CNC samples processed with oxidation at a sawdust–to–APS ratio of 1:40 and APS concentration of 1 M (Figure 7(a)–(b)), and samples processed with a combination of oxidation and acid hydrolysis at a sawdust–to–APS ratio of 1:30 and APS concentration of 2 M (Figure 7(c)–(d)). In Figure 7(a)–(b), the morphology of the nanofibrils in a rod–like structure is observed, which remains intertwined with persistent amorphous regions [38]. The direct oxidation process using APS only removes lignin and hemicellulose and breaks down cellulose fibers into microfibrils/ nanofibrils. However, the amorphous regions remain intact [63]. As a result, the

produced microfibril/ nanofibril structure remains interconnected and elongated, but does not yet meet the desired CNC specifications. This indicates that CNCs cannot be obtained from Meranti sawdust using a single–step method (oxidation process). Meranti cellulose fibers contain more than 20% lignin [32] and have a linear structure that binds cellulose through hydrogen bonds [64], [65]. These hydrogen bonds cause the cellulose surface to be covered and obstructed, making it difficult for the radicals generated by APS to oxidize cellulose into CNCs [1]. These findings confirm that oxidation alone is insufficient to break down cellulose fibers into CNCs effectively, requiring additional steps to more thoroughly isolate crystalline cellulose.

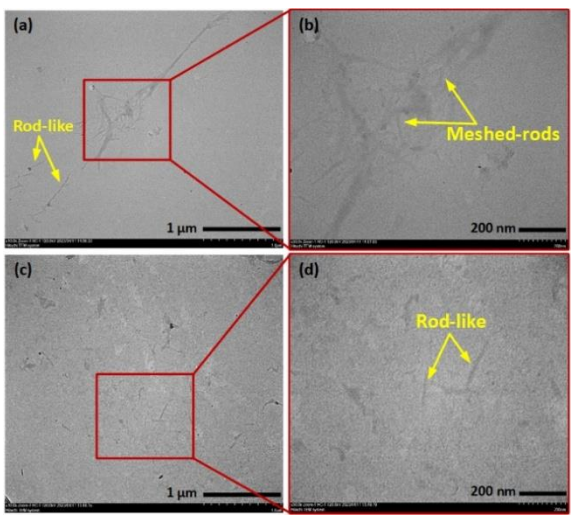

Figure 7: TEM analysis results for (a–b) Oxidation process 1:40 1M, (c–d) Oxidation and acid hydrolysis process 1:30 2M.

In Figure 7(c)–(d), the morphology of the CNCs produced after oxidation and acid hydrolysis shows a rod–like structure with smaller particle sizes down to the nanometer scale, forming CNCs. This result is consistent with the findings of Sacui *et al.*, [66] and Thompson *et al.*, [67], who reported that CNCs produced from wood exhibit a rod–like structure and high crystallinity. Oxidation followed by acid hydrolysis proved effective in breaking down the amorphous structure, allowing for the formation of CNCs with smaller and more uniform sizes, which is a crucial step in enhancing the application of CNC–based materials.

Figure 8 shows the particle size distribution resulting from the oxidation process and the combination of oxidation–acid hydrolysis. Particle dimensions (length and width) were measured using ImageJ from TEM micrographs after calibration with the scale bar. To minimize selection bias, particles were selected randomly from the TEM fields–of–view. Results are reported as mean ± standard deviation based on the number of measured particles (n), which is specified for each condition.

For the oxidation–only condition (1M APS, sawdust–to–APS ratio of 1:40), the particle length of the resulting CNCs is approximately 379.98 ± 47.87 nm and the width is 23.94 ± 0.37 nm (Figures 8(a)–(b)), with an aspect ratio (L/D) of approximately 15.87 ± 2.01, based on n = 28 measured particles. These particles are larger and show a broader size distribution compared to the CNCs produced after oxidation and acid hydrolysis. In this oxidation process, although the cellulose fibers are broken down into microfibrils and nanofibrils, many amorphous regions remain intact, leading to the formation of larger aggregates. This is consistent with previous findings that indicate lower APS concentration oxidation is less effective in producing CNCs with smaller and more uniformly distributed sizes [68].

In contrast, in the oxidation and acid hydrolysis condition (2 M APS, sawdust–to–APS ratio of 1:30), the particle length of the resulting CNCs is smaller, approximately 188.71 ± 5.01 nm with a width of 26.79 ± 1.72 nm (Figure 8(c)–(d)), and an aspect ratio (L/D) of approximately 7.04 ± 0.49, based on n = 67 measured CNCs. The smaller particle size indicates that acid hydrolysis plays a significant role in improving the particle size and size distribution of the CNCs. By removing most of the amorphous regions from the cellulose, the acid hydrolysis process results in more uniform and smaller particles, which are highly desirable for nanomaterial applications in various fields, including composite materials and biosensors [69], [70].

This TEM–derived length scale is consistent with conventional wood–CNC production via concentrated sulfuric acid hydrolysis of purified pulps as performed by Chen *et al*., who quantified a length–weighted average crystal length spanning ~130.5–228.2 nm across representative reaction conditions. Chen *et al.,* further noted that at lower acid concentration (56 wt%), insufficient depolymerization yielded more nanofibril–like particles rather than a well–defined CNC morphology [52].

The increase in crystallinity observed in the samples processed with oxidation and acid hydrolysis

(APS concentration of 2 M) is also directly related to the reduction in CNC particle size. The acid hydrolysis process improves the quality of the CNCs by increasing crystallinity and reducing particle size through the breakdown of amorphous regions, supporting previous findings that high crystallinity in CNCs contributes to enhanced mechanical and thermal properties [1]. Thus, the oxidation process followed by acid hydrolysis demonstrates higher efficiency in producing CNCs with a narrower size distribution and higher quality [8].

The aspect ratio (L/D) is an important parameter for application design, because it influences reinforcement potential and processing behavior. In the oxidation–only sample, the higher aspect ratio reflects longer fibrillar/aggregated structures, whereas the combined oxidation–acid hydrolysis condition yields shorter rods with more consistent dimensions within the measured population [71]. The structural characteristics of the CNCs obtained from Meranti sawdust are relevant to several advanced material applications. For polymer nanocomposites, the combination of high crystallinity and rod–like geometry can support efficient load transfer and reinforcement, while a moderate aspect ratio may ease processing compared with highly fibrillar/high–aspect ratio particles [30], [31]. For coatings and thin films, nanoscale dimensions and a relatively narrow size distribution under the optimized condition can contribute to more uniform film formation and surface coverage, supporting barrier–oriented coating/film development [72], [73]. Compared with CNCs produced from purified/bleached cellulose sources, sawdust–derived CNCs may face greater feedstock variability and a higher likelihood of residual non–cellulosic components (e.g., lignin/extractives), which can influence color, surface chemistry consistency, and reproducibility [74], [75]. Nevertheless, the present results indicate that high–lignin sawdust can still yield CNCs with structural characteristics within the typical range reported for wood–based CNCs [30], [76].

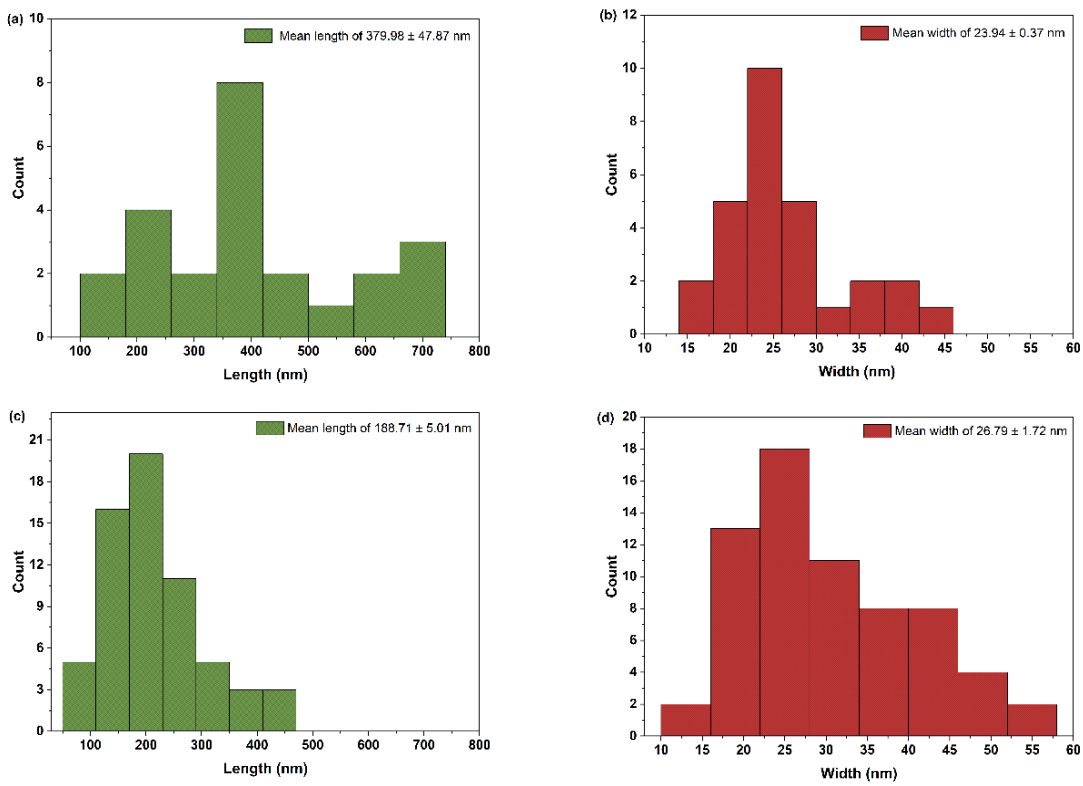

Figure 8: Particle size for (a)–(b) Oxidation process 1:40 1M, (c)–(d) Oxidation and acid hydrolysis process 1:30 2M.

4 Conclusions

This study demonstrates the feasibility of producing cellulose nanocrystals (CNCs) from high–lignin Meranti sawdust using a two–step APS oxidation followed by sulfuric–acid hydrolysis without prior alkaline pulping or bleaching. Under the optimised condition (2 M APS and a sawdust–to–APS ratio of 1:30, w/v), the resulting CNCs exhibited the highest crystallinity index (72%) and nanoscale, rod–like morphology, with an average particle size of 188.71 ± 5.01 nm. Acid hydrolysis facilitated the removal of disordered regions and the release of CNCs. From a scalability perspective, this route involves APS consumption governed by molarity and liquid–to–solid ratio, a cumulative processing time of 7 h oxidation and 2 h hydrolysis plus washing/neutralisation to pH ~6, and generates sulfate–containing aqueous effluent from persulfate/acid usage and washing steps. Compared with conventional CNC production routes that typically involve alkaline pulping and multistage bleaching prior to acid hydrolysis, the proposed APS/acid route eliminates dedicated alkali/bleaching steps, thereby potentially reducing process complexity and avoiding bleaching–specific waste streams. In this study, the chemical inputs are mainly APS and sulfuric acid, while the principal liquid waste is sulfate–containing wash liquor generated during quenching, washing, and neutralisation. With routine neutralisation and wastewater management, this streamlined chemistry offers a practical pathway for converting high–lignin sawdust into CNCs while limiting the need for additional pulping/bleaching chemicals.

Acknowledgments

This work was supported by Lembaga Penelitian dan Pengabdian Kepada Masyarakat (LPPM) Universitas Riau via skema Riset Mandatory (RIMA) (Grant number: 16917/UN19.5.1.3/AL.04/2024).

Author Contributions

A.A.: conceptualization, funding acquisition, and methodology; H.T.: data analysis; D.S.: investigation, writing an original draft; I.O.S.: investigation, writing an original draft; C.: project administration, research design; S.P.U.: data curation; H.A.M.: supervision; M.M.R.: software; K.J.: writing—reviewing and editing; Z.T.J.: visualization, resources. All authors have read and agreed to the published version of the manuscript.

Conflicts of Interest

The authors declare no conflict of interest.

Declaration of generative AI and AI-assisted technologies in the writing process

The authors declare no use of AI and AI-assisted tool.

References

[1] N. T. U. Culsum, C. Melinda, I. Leman, A. Wibowo, and Y. W. Budhi, "Isolation and characterization of cellulose nanocrystals (CNCs) from industrial denim waste using ammonium persulfate," *Materials Today Communications*, vol. 26, Mar. 2021, Art. no. 101817, doi: 10.1016/j.mtcomm.2020.101817.

[2] A. Farooq et al., "Cellulose from sources to nanocellulose and an overview of synthesis and properties of nanocellulose/zinc oxide nanocomposite materials," *International Journal of Biological Macromolecules*, vol. 154, pp. 1050–1073, Jul. 2020, doi: 10.1016/j.ijbiomac.2020.03.163.

[3] R. K. Mishra, A. Sabu, and S.K. Tiwari, "Materials chemistry and the futurist eco-friendly applications of nanocellulose: Status and prospect," *Journal of Saudi Chemical Society*, vol. 22, no.8, pp. 949–978, Des. 2018, doi: 10.1016/j.jscs.2018.02.005.

[4] N. Raghav, M. R. Sharma, and J. F. Kennedy, "Nanocellulose: A mini-review on types and use in drug delivery systems," *Carbohydrate Polymer Technologies and Applications*, vol. 2, Des. 2021, Art. no. 100031, doi: 10.1016/j.carpta.2020.100031.

[5] A. Elmgerbi, I.A. Askar, A. Fine, G. Thonhauser, and R. Ashena, "Cellulose nanocrystals (CNCs) as a potential additive for improving API class G cement performance: An experimental study," *Natural Gas Industry B*, vol. 10, no. 3, pp. 233–244, May 2023, doi: 10.1016/j.ngib.2023.05.001.

[6] W. Somphol *et al.,* "Extraction of cellulose nanocrystals and nanofibers from rubber leaves and their impacts on natural rubber properties," *Applied Science and Engineering Progress*, vol.

17, no. 2, Nov. 2024, Art. no. 7281, doi: 10.14416/j.asep.2023.11.010.

[7] S. Garriba, H.S. Jailani, and C.K.A. Pandian, "Characterization of mechanical, viscoelastic, thermal properties of epoxy/*Mariscus ligularis* fiber composites," *Fibers and Polymers*, vol. 25, pp. 3975–3994, Oct. 2024, doi : 10.1007/s12221-024-00707-0.

[8] Y. Zhang et al., "Preparation methods of cellulose nanocrystal and its application in treatment of environmental pollution: A mini-review," *Colloid and Interface Science Communications*, vol. 53, Mar. 2023, Art. no. 100707, doi: 10.1016/j.colcom.2023.100707.

[9] A. A. Kacaribu, R. Rahmi, J. Julinawati, H. Fathana, M. Reza, and M. Iqhramullah, "Preparation and characterization of cellulose film from velvet tamarind rind (*Dialium indum* L.) for food packaging," *Applied Science and Engineering Progress*, vol. 18, no. 3, Mar. 2025, Art. no. 7724, doi: 10.14416/j.asep.2025.03.006.

[10] S. Yu, J. Sun, Y. Shi, Q. Wang, J. Wu, and J. Liu, "Nanocellulose from various biomass wastes: Its preparation and potential usages towards the high value-added products," *Environmental Science and Ecotechnology*, vol. 5, Mar. 2021, Art no. 100077, doi: 10.1016/j.ese.2020.100077.

[11] R. Moriana, F. Vilaplana, and M. Ek, "Cellulose nanocrystals from forest residues as reinforcing agents for composites: A study from macro- to nano-dimensions," *Carbohydrate Polymers*, vol. 139, pp. 139–149, Mar. 2016, doi: 10.1016/j.carbpol.2015.12.020.

[12] S. B. A. Hamid, Md. A. Amin, and M. E. Ali, "Zeolite supported ionic liquid catalyst for the synthesis of nano-cellulose from palm tree biomass," *Advanced Materials Research*, vol. 925, pp. 52–56, Apr. 2014, doi: 10.4028/www.scientific.net/AMR.925.52.

[13] M. Asadnia and M. Sadat-Shojai, "Recent perspective of synthesis and modification strategies of cellulose nanocrystals and cellulose nanofibrils and their beneficial impact in scaffold-based tissue engineering: A review," *International Journal of Biological Macromolecules*, vol. 293, Mar. 2025, Art. no. 139409, doi: 10.1016/j.ijbiomac.2024.139409.

[14] M. N. F. Norrrahim et al., "Isolation and functionalization of nanocellulose-based bamboo origin," in *Bamboo-Based Polymer Composites*, N. Norizan, S. M. Sapuan, and M. N. F. Norrrahim, Ed. Sawston, UK: Woodhead Publishing, 2025, pp. 61–85, doi: 10.1016/B978-0-443-33445-0.00004-3.

[15] J. E. Andrew, J. Johakimu, P. Lekha, M. E. Gibril, and B. B. Sitholé, "Beneficiation of sawdust waste material within the context of an integrated forest biorefinery mill: Kraft and prehydrolysis kraft pulping properties," in *Opportunities for Biomass and Organic Waste Valorisation*, L. Godfrey, J. F. Görgens, and H. Roman, Ed. London, UK: Routledge, Jul. 2018, pp. 123–139, doi: 10.4324/9780429201998-12.

[16] Y. Liu et al., "Modified ammonium persulfate oxidations for efficient preparation of carboxylated cellulose nanocrystals," *Carbohydrate Polymers*, vol. 229, Feb. 2020, Art. no. 115572, doi: 10.1016/j.carbpol.2019.115572.

[17] T. Saito, Y. Okita, T.T. Nge, J. Sugiyama, and A. Isogai, "TEMPO-mediated oxidation of native cellulose: Microscopic analysis of fibrous fractions in the oxidized products," *Carbohydrate Polymers*, vol. 65, no. 4, pp. 435–440, Sep. 2006, doi: 10.1016/j.carbpol.2006.01.034.

[18] J. Gröndahl, K. Karisalmi, and J. Vapaavuori, "Micro- and nanocelluloses from non-wood waste sources; processes and use in industrial applications," *Soft Matter*, vol. 17, no. 43, pp. 9842–9858, Oct. 2021, doi: 10.1039/D1SM00958C.

[19] M. H. Hing, M. H. M. Pisal, N. A. A. Sezali, H. L. Ong, and R.-A. Doong, "Physicochemical properties of industrial wood waste-derived cellulose nanofibrils," in *Proceedings of the 3rd International Conference on Biomass Utilization and Sustainable Energy*, 2024, pp. 193–204, doi: 10.1007/978-981-99-9164-8_17.

[20] D. M. do Nascimento *et al.,* "A comprehensive approach for obtaining cellulose nanocrystal from coconut fiber. Part I: Proposition of technological pathways," *Industrial Crops and Products*, vol. 93, pp. 66–75, Des. 2016, doi: 10.1016/j.indcrop.2015.12.078.

[21] E. Scopel, L. O. Pinto, and C. A. Rezende, "Single-step bleaching versus organosolv-bleaching of sugarcane bagasse: tuning TEMPO-oxidized nanocellulose morphology via delignification strategy," *International Journal of Biological Macromolecules*, vol. 25, Dec.

2025, Art. no. 147296, doi: 10.1016/j.ijbiomac.2025.147296.
[22] J. Xie et al., "New ternary deep eutectic solvents with cycle performance for efficient pretreated radiata pine forming to lignin containing cellulose nanofibrils," *Chemical Engineering Journal*, vol. 451, no. 1, Jan. 2023, Art. no. 138591, doi: 10.1016/j.cej.2022.138591.
[23] P. Baranitharan et al., "Chemically pretreated biomass conversion for biorefinery: A review of current trends," *Korean Chemical Engineering Research*, vol. 63, no. 2, pp. 145–164, Mar. 2025, doi: 10.9713/kcer.2025.63.2.105104.
[24] Z. Chen, Z. Xie, and H. Jiang, "Extraction of the cellulose nanocrystals via ammonium persulfate oxidation of beaten cellulose fibers," *Carbohydrate Polymers*, vol. 318. Oct. 2023, Art no. 121129, doi: 10.1016/j.carbpol.2023.121129.
[25] A. C. W. Leung et al., "Characteristics and properties of carboxylated cellulose nanocrystals prepared from a novel one-step procedure," *Small*, vol. 7, no. 3, pp. 302–305, Des. 2010, doi: 10.1002/smll.201001715.
[26] Y. Wu, F. Cao, H. Jiang, and Y. Zhang, "Carboxyl cellulose nanocrystal extracted from hybrid poplar residue," *Bioresources*, vol. 12, no. 4, pp. 8775–8785, Oct. 2017, doi: 10.15376/biores.12.4.8775-8785.
[27] Z. Q. Zhao and X. P. Ouyang, "Effect of oxidation on the structures and properties of lignin," *Advanced Materials Research*, vol. 550–553, pp. 1208–1213, Jul. 2012, doi: 10.4028/www.scientific.net/AMR.550-553.1208.
[28] M. Davaritouchaee and S. Chen, "Persulfate oxidizing system for biomass pretreatment and process optimization," *Biomass Bioenergy*, vol. 116, pp. 249–258, Sep. 2018, doi: 10.1016/j.biombioe.2018.06.021.
[29] L. H. Zaini et al., "Effect of ammonium persulfate concentration on characteristics of cellulose nanocrystals from oil palm frond," *Journal of the Korean Wood Science and Technology*, vol. 47, no. 5, pp. 597–606, Sep. 2019, doi: 10.5658/WOOD.2019.47.5.597.
[30] R. J. Moon, A. Martini, J. Nairn, J. Simonsen, and J. Youngblood, "Cellulose nanomaterials review: structure, properties and nanocomposites," *Chemical Society Reviews*. vol. 40, no. 7, Mar. 2011, Art no. 3941, doi: 10.1039/c0cs00108b.
[31] Y. Habibi, L. A. Lucia, and O. J. Rojas, "Cellulose nanocrystals: Chemistry, self-Assembly, and applications," *Chemical Reviews*, vol. 110, no. 6, pp. 3479–3500. Mar. 2010, doi: 10.1021/cr900339w.
[32] Z. S. Ahmad, M. S. A. Munaim, and F. M. Said, "Characterization of *meranti* wood sawdust and removal of lignin content using pre-treatment process," in *Proceedings of the National Conference for Postgraduate Research (NCON-PGR 2016)*, 2016, pp. 598–606.
[33] N. A. M. Razali, F. A. Aziz, and S. A. Rahman, "Preliminary preparation and characterization studies of cellulose from Merbau (*intsia bijuga*)," *Advanced Materials Research*, vol. 620, pp. 314–319, Dec. 2012, doi: 10.4028/www.scientific.net/AMR.620.314.
[34] G. Kandhola et al., "Impact of species-based wood feedstock variability on physicochemical properties of cellulose nanocrystals," *Cellulose*, vol. 29, pp. 8213–8228, Oct. 2022, doi: 10.1007/s10570-022-04762-9.
[35] A. R. Nafisah, D. Rahmawati, and F. M. Tarmidzi, "Synthesis of cellulose nanofiber from palm oil empty fruit bunches using acid hydrolysis method," *Indonesian Journal of Chemical Science*, vol. 11, no. 3, pp. 233–240, Nov. 2022, doi: 10.15294/ijcs.v11i3.55936.
[36] S. Nam, A. D. French, B. D. Condon, and M. Concha, "Segal crystallinity index revisited by the simulation of X-ray diffraction patterns of cotton cellulose Iβ and cellulose II," *Carbohydrate Polymers*, vol. 135, pp. 1–9, Jan. 2016, doi: 10.1016/j.carbpol.2015.08.035.
[37] S. Fatimah, R. Ragadhita, D. Fitria, A. Husaeni, A. Bayu, and D. Nandiyanto, "How to calculate crystallite size from X-ray diffraction (XRD) using Scherrer method," *ASEAN Journal of Science and Engineering*, vol. 2, no. 1, pp. 65–76, Jun. 2021, doi: 10.17509/ajse.v2i1.37647.
[38] T. I. Shaheen and H. E. Emam, "Sono-chemical synthesis of cellulose nanocrystals from wood sawdust using Acid hydrolysis," *International Journal of Biological Macromolecules*, vol. 107, no. 2, pp. 1599–1606, Feb. 2018, doi: 10.1016/j.ijbiomac.2017.10.028.
[39] J. Guo, X. Guo, S. Wang, and Y. Yin, "Effects of ultrasonic treatment during acid hydrolysis on the yield, particle size and structure of cellulose nanocrystals," *Carbohydrate Polymers*, vol. 135, pp. 248–255, Jan. 2016, doi: 10.1016/j.carbpol.2015.08.068.

[40] M. M. Bashar, H. Zhu, S. Yamamoto, and M. Mitsuishi, "Highly carboxylated and crystalline cellulose nanocrystals from jute fiber by facile ammonium persulfate oxidation," *Cellulose*, vol. 26, pp. 3671–3684, Apr. 2019, doi: 10.1007/s10570-019-02363-7.

[41] Q. Lu, W. Lin, L. Tang, S. Wang, X. Chen, and B. Huang, "A mechanochemical approach to manufacturing bamboo cellulose nanocrystals," *Journal of Materials Science*, vol. 50, pp. 611–619, Jan. 2015, doi: 10.1007/s10853-014-8620-6.

[42] S. Wang, Q. Wang, and Y. Kai, "Cellulose nanocrystals obtained from microcrystalline cellulose by p-toluene sulfonic acid hydrolysis, NaOH and ethylenediamine treatment," *Cellulose*, vol. 29, pp. 1637–1646, Feb. 2022, doi: 10.1007/s10570-021-04409-1.

[43] H. A. Silvério, W. P. Flauzino Neto, N. O. Dantas, and D. Pasquini, "Extraction and characterization of cellulose nanocrystals from corncob for application as reinforcing agent in nanocomposites," *Industrial Crops Products*, vol. 44, pp. 427–436, Jan. 2013, doi: 10.1016/j.indcrop.2012.10.014.

[44] S. R. Stoyanov, O. Lyubimova, S. Gusarov, and A. Kovalenko, "Computational modeling of the structure relaxation and dispersion thermodynamics of pristine and modified cellulose nanocrystals in solution," *Nordic Pulp & Paper Research Journal*, vol. 29, no. 1, pp. 144–155, Jan. 2014, doi: 10.3183/npprj-2014-29-01-p144-155.

[45] A.A. Al-Tabbakh, N. Karatepe, A.B. Al-Zubaidi, A. Benchaabane, and N.B. Mahmood, "Crystallite size and lattice strain of lithiated spinel material for rechargeable battery by X-ray diffraction peak-broadening analysis," *International Journal of Energy Research*, vol. 43, no. 5, pp. 1903–1911, Feb. 2019, doi: 10.1002/er.4390.

[46] M. Cheng et al., "Efficient extraction of carboxylated spherical cellulose nanocrystals with narrow distribution through hydrolysis of lyocell fibers by using ammonium persulfate as an oxidant," *Journal of Materials Chemistry A*, vol. 2, no. 1, pp. 251–258, Oct. 2014, doi: 10.1039/C3TA13653A.

[47] S.K. Mudedla et al., "Effect of oxidation on cellulose and water structure: A molecular dynamics simulation study," *Cellulose*, vol. 28, pp. 3917–3933, May 2021, doi: 10.1007/s10570-021-03751-8.

[48] S. W. Suciyati, P. Manurung, J. Junaidi, and R. Situmeang, "Cladophora nanocrystalline cellulose: Structure and morphology," *AIP Conference Proceedings*, vol. 2970, Sep. 2024, Art. no. 020008, doi: 10.1063/5.0209073.

[49] M. S. Rana *et al.,* "Morphological, spectroscopic and thermal analysis of cellulose nanocrystals extracted from waste jute fiber by acid hydrolysis," *Polymers (Basel)*, vol. 15, no. 6, Mar. 2023, Art. no. 1530, doi: 10.3390/polym15061530.

[50] H. Khanjanzadeh and B.-D. Park, "Optimum oxidation for direct and efficient extraction of carboxylated cellulose nanocrystals from recycled MDF fibers by ammonium persulfate," *Carbohydrate Polymers*, vol. 251, Jan. 2021, Art. no. 117029, doi: 10.1016/j.carbpol.2020.117029.

[51] Y. Hu, L. Tang, Q. Lu, S. Wang, X. Chen, and B. Huang, "Preparation of cellulose nanocrystals and carboxylated cellulose nanocrystals from borer powder of bamboo," *Cellulose,* vol. 21, pp. 1611–1618, Jun. 2014, doi: 10.1007/s10570-014-0236-0.

[52] L. Chen, Q. Wang, K. Hirth, C. Baez, U. P. Agarwal, and J. Y. Zhu, "Tailoring the yield and characteristics of wood cellulose nanocrystals (CNC) using concentrated acid hydrolysis," *Cellulose*, vol. 22, pp. 1753–1762. May. 2015, doi: 10.1007/s10570-015-0615-1

[53] T. Kawakubo et al., "Analysis of exposed cellulose surfaces in pretreated wood biomass using carbohydrate-binding module (CBM)–cyan fluorescent protein (CFP)," *Biotechnology and Bioengineering*, vol. 105, no. 3, pp. 499–508, Feb. 2010, doi: 10.1002/bit.22550.

[54] E. Gicquel et al., "Impact of sonication on the rheological and colloidal properties of highly concentrated cellulose nanocrystal suspensions," *Cellulose*, vol. 26, pp. 7619–7634, Sep. 2019, doi: 10.1007/s10570-019-02622-7.

[55] D. B. Effendi, N. H. Rosyid, A. B. D. Nandiyanto, and A. Mudzakir, "Review: sintesis nanoselulosa," *Jurnal Integrasi Proses*, vol. 5, no. 2, pp. 61–74, Jun. 2015.

[56] E. Widiastuti and A. Marlina, "Optimasi pembuatan nanoselulosa dari rumput alang-alang," *Jurnal Fluida*, vol. 13, no. 2, pp. 59–64, Nov. 2020, doi: 10.35313/fluida.v13i2.2249.

[57] N. F. Vasconcelos et al., "Bacterial cellulose nanocrystals produced under different hydrolysis conditions: Properties and morphological features," *Carbohydrate Polymers*, vol. 155, pp. 425–431, Jan. 2017, doi: 10.1016/j.carbpol.2016.08.090.

[58] M. H. Gehlen, "Kinetics of autocatalytic acid hydrolysis of cellulose with crystalline and amorphous fractions," *Cellulose*, vol. 17, pp. 245–252, Apr. 2010, doi: 10.1007/s10570-009-9385-y.

[59] M. Martínez-Sanz, A. Lopez-Rubio, and J.M. Lagaron, "Optimization of the nanofabrication by acid hydrolysis of bacterial cellulose nanowhiskers," *Carbohydrate Polymers*, vol. 85, no. 1, pp. 228–236, Apr. 2011, doi: 10.1016/j.carbpol.2011.02.021.

[60] Y. Nishiyama, J. Sugiyama, H. Chanzy, and P. Langan, "Crystal structure and hydrogen bonding system in cellulose I α from synchrotron X-ray and neutron fiber diffraction," *Journal of the American Chemical Society*, vol. 125, no. 47, pp. 14300–14306, Nov. 2003, doi: 10.1021/ja037055w.

[61] A. Solikhin, Y. S. Hadi, M. Y. Massijaya, and S. Nikmatin, "Morphological, chemical, and thermal characteristics of nanofibrillated cellulose isolated using chemo-mechanical methods," *Makara Journal of Science*, vol. 21, no. 2, pp. 59–68, Jul. 2017, doi: 10.7454/mss.v21i2.6085.

[62] N. Rambabu, S. Panthapulakkal, M. Sain, and A.K. Dalai, "Production of nanocellulose fibers from pinecone biomass: Evaluation and optimization of chemical and mechanical treatment conditions on mechanical properties of nanocellulose films," *Industrial Crops and Products*, vol. 83, pp. 746–754, May, 2016, doi: 10.1016/j.indcrop.2015.11.083.

[63] K. Y. Goh, Y. C. Ching, C. H. Chuah, L. C. Abdullah, and N.S. Liou, "Individualization of microfibrillated celluloses from oil palm empty fruit bunch: comparative studies between acid hydrolysis and ammonium persulfate oxidation," *Cellulose*, vol. 23, pp. 379–390, Feb. 2016, doi: 10.1007/s10570-015-0812-y.

[64] R. Parthasarathi, G. Bellesia, S. P. S. Chundawat, B. E. Dale, P. Langan, and S. Gnanakaran, "Insights into hydrogen bonding and stacking interactions in cellulose," *The Journal of Physical Chemistry A*, vol. 115, no. 49, pp. 14191–14202, Des. 2011, doi: 10.1021/jp203620x.

[65] C. M. Lee, J. D. Kubicki, B. Fan, L. Zhong, M. C. Jarvis, and S. H. Kim, "Hydrogen-bonding network and OH stretch vibration of cellulose: Comparison of computational modeling with polarized IR and SFG spectra," *The Journal of Physical Chemistry B*, vol. 119, no. 49, pp. 15138–15149, Des. 2015, doi: 10.1021/acs.jpcb.5b08015.

[66] I. A. Sacui et al., "Comparison of the properties of cellulose nanocrystals and cellulose nanofibrils isolated from bacteria, tunicate, and wood processed using acid, enzymatic, mechanical, and oxidative methods," *ACS Applied Materials & Interfaces*, vol. 6, no. 9, pp. 6127–6138, May. 2014, doi: 10.1021/am500359f.

[67] L. Thompson, M. Nikzad, I. Sbarski, J. Azadmanjiri, J. Ren, and A. Yu, "Production of cellulose nanocrystals from australian wood sources," *Journal of Nanoscience and Nanotechnology,* vol. 20, no. 9, pp. 5642–5647, Sep. 2020, doi: 10.1166/jnn.2020.17879.

[68] N. L. Indirasetyo and Kusmono, "Isolation and properties of cellulose nanocrystals fabricated by ammonium persulfate oxidation from *sansevieria trifasciata* fibers," *Fibers*, vol. 10, no. 7, Jul. 2022, Art. no. 61, doi: 10.3390/fib10070061.

[69] W. L. Lim, A. A. N. Gunny, and F. H. Kasim, "Overview of cellulose nanocrystals: extraction, physicochemical properties and applications," *IOP Conference Series: Materials Science and Engineering,* vol. 670, no. 1, Nov. 2019, Art. no. 012058, doi: 10.1088/1757-899X/670/1/012058.

[70] K. M. Vanhatalo and O. P. Dahl, "Effect of mild acid hydrolysis parameters on properties of microcrystalline cellulose," *Bioresources*, vol. 9, no. 3, pp. 4729-4740, Jun. 2014, doi: 10.15376/biores.9.3.4729-4740.

[71] M. Kröger et al., "Surface-vinylated cellulose nanocrystals as cross-linkers for hydrogel composites," *Biomacromolecules*, vol. 26, no. 4, pp. 2282–2292, Apr. 2025, doi: 10.1021/acs.biomac.4c01619.

[72] M. Guivier, G. Almeida, S. Domenek, and C. Chevigny, "Resilient high oxygen barrier multilayer films of nanocellulose and polylactide," *Carbohydrate Polymers*, vol. 312, Jul. 2023, Art. no. 120761, doi: 10.1016/j.carbpol.2023.120761.

[73] A. Ferrer, L. Pal, and M. Hubbe, "Nanocellulose in packaging: Advances in barrier layer technologies," *Industrial Crops and Products*, vol. 95, pp. 574–582, Jan. 2017, doi: 10.1016/j.indcrop.2016.11.012.

[74] E. Rojo et al., "Comprehensive elucidation of the effect of residual lignin on the physical, barrier, mechanical and surface properties of nanocellulose films," *Green Chemistry*, vol. 17, no. 3, pp. 1853–1866, Jan. 2015, doi: 10.1039/C4GC02398F.

[75] R. O. Almeida, A. Ramos, E. Kimiaei, M. Österberg, T. C. Maloney, and J. A. F. Gamelas, "Improvement of the properties of nanocellulose suspensions and films by the presence of residual lignin," *Cellulose*, vol. 31, no. 18, pp. 10951–10967, Dec. 2024, doi: 10.1007/s10570-024-06222-y.

[76] M. Raza and B. Abu-Jdayil, "Cellulose nanocrystals from lignocellulosic feedstock: A review of production technology and surface chemistry modification," *Cellulose*, vol. 29, no. 2, pp. 685–722, Jan. 2022, doi: 10.1007/s10570-021-04371-y.